AIAA JOURNAL
Vol. 39, No. 7, July 2001

# Locating Delaminations in Composite Beams Using Gradient Techniques and a Genetic Algorithm

C. Harrison*
*GKN Westland Helicopters, Ltd., Yeovil, Somerset, England BA20 2YB, United Kingdom*
and
R. Butler†
*University of Bath, Bath, England BA2 7AY, United Kingdom*

**A method of locating delaminations within composite beams is presented. The method compares the experimental natural frequencies and mode shapes of a delaminated beam with those predicted by an analytical model. The differences are quantified by an objective function, which is minimized using a numerical optimization technique. When the difference between the analytically produced modal parameters and those measured experimentally is minimized, the damage is said to have been located. A simple model, based on the static deflection of a cantilever beam, is developed to obtain an estimate for the effective shear rigidity of the delaminated area, and this is incorporated into the dynamic stiffness method. The damage is located using a two-stage optimization process. First, the differences in the analytical and experimental bending frequencies and mode shapes are minimized by altering the material properties and boundary conditions of the model. Once the differences have been minimized for an undamaged beam, damage is located by altering the number, size, and location of delaminations within the beams. Results are obtained and compared using two different optimization procedures: a gradient-based optimization procedure and a genetic algorithm.**

## Introduction

DELAMINATIONS can cause significant reductions in the load-bearing properties of composite laminates and can be difficult or impossible to detect with the naked eye. Hence, nondestructive testing (NDT) of composite materials receives considerable interest in the materials and structures community.

Commonly used NDT techniques include ultrasonic scanning, transient thermography, and x radiography, which require portable equipment and can be slow to use and, therefore, costly. Modal analysis offers significant advantages over common NDT techniques such as those mentioned. Modal parameters such as frequency and damping measurements can be made at one point of the structure. Therefore, a time-consuming scan of the whole structure is not necessary. For this reason, a number of modal NDT techniques have been developed (for example, see Ref. 1). Many of the methods found in the relevant literature use optimization techniques, although most model damage as reductions in stiffness or mass.[2,3] Relatively few researchers have concentrated on delaminations.[4]

This paper presents a method of detecting and locating delaminations within laminated composite beams, using experimentally obtained frequencies and mode shapes. In this method, the dynamic stiffness method (DSM) is used to model the free vibration of the laminates.[5] First, the model of the undamaged laminate is compared to the behavior of undamaged beams found experimentally, and a numerical optimization technique is used to update the model. This accurately determines the material properties and support conditions of the cantilever. The beam is then damaged, and the experimental vibration of the beam is measured. The damage is then located using either a gradient-based optimizer or a genetic algorithm (GA) to vary the location and size of the delaminations in the model until the difference between the experimental response and analytical prediction is minimized. A delamination is assumed to affect only the shear rigidity of the beam, and, hence, only the bending modes of vibration are used in this process.

This paper outlines the theoretical model of a delaminated beam and the methods used to locate delaminations using two numerical optimizers. Finally, the methods are applied to locate delaminations within experimental composite beams.

## Theory

### Delamination Model

The DSM is used to model the free vibration of a shear deformable composite beam with bending–torsion coupling.[5] The DSM follows from the exact solutions of the governing differential equations of motion of the beam. Because the beam is assumed to have a continuous distribution of mass and rigidity along its length, an infinite number of degrees of freedom are allowed for. Therefore, as many natural frequencies as desired can be obtained without increasing the number of elements in the model. This is in contrast to finite element (FE) methods, which discretize the model by lumping distributed masses at nodes. Only a finite number of modes of vibration can be obtained, this number being the number of degrees of freedom of the model. In addition, an FE solution becomes more inaccurate for higher-order modes, and increased accuracy can only be obtained by increasing the number of nodes of the structure, which increases the analysis time. Therefore, the DSM is much more suitable to numerical optimization, which requires repeated calculation of the dynamic properties of the structure.

To apply the DSM, a beam is split up along its length into elements with known material and geometric properties. A delaminated element is assumed to have a reduced shear rigidity. The shear rigidity of a delaminated section is calculated using a static beam model.

In the static beam model, a delamination is modeled as two or more beams stacked on top of one another, with rigidly connected endfaces. This, therefore, represents a beam with full-length and full-width debonds running parallel to the $Y$ axis. The reduction in shear rigidity is calculated via a tip-loaded cantilever beam, which has constant shear force acting along its length. Figure 1 shows such a beam with $n-1$ delaminations, giving sublaminates 1 through $n$.

From the free body diagram in Fig. 1, resolving horizontally and taking moments about the neutral axis of the undelaminated laminate for points 1 and 2 gives

$$\sum_{i=1}^{n} M_{i_1} + \sum_{i=1}^{n} P_{i_2} \bar{z}_i = M_1 \tag{1}$$

$$\sum_{i=1}^{n} M_{i_2} + \sum_{i=1}^{n} P_{i_2} \bar{z}_i = M_2 \tag{2}$$

Received 8 August 2000; revision received 2 November 2000; accepted for publication 10 November 2000. 

*Dynamics Design Engineer, Rotor Technology Department.
†Senior Lecturer, Department of Mechanical Engineering.

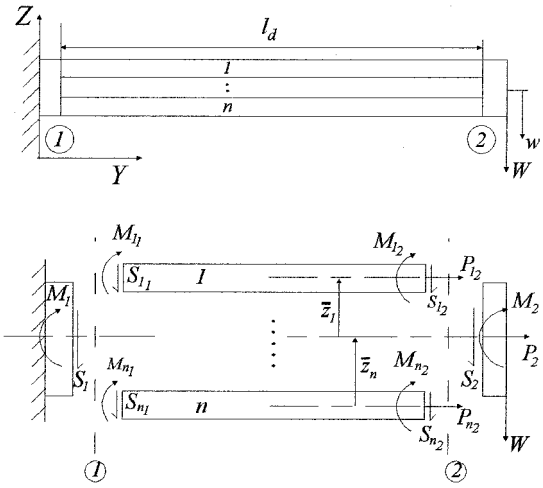


**Fig. 1 Delaminated beam section of length $l_d$ with tip load $W$.**

The bending moment varies linearly with distance along the laminate, that is, $M = M_1 - Sy$, and the shear force remains constant along the beam, that is, $S_1 = S_2 = S$. Therefore, Eq. (2) can be rewritten as

$$\sum_{i=1}^{n} M_{i_1} - \sum_{i=1}^{n} S_i l_d + \sum_{i=1}^{n} P_{i_2}\bar{z}_i = M_1 - Sl_d \tag{3}$$

Under the assumption that the shear deflection within sublaminates is negligible, the bending deflection and gradient of each sublaminate at point 2 is calculated using engineers bending theory:

$$w_i' = -\frac{M_{i_1} l_d}{(EI)_i} + \frac{S_i l_d^2}{2(EI)_i} + K_{BA_i} P_{i_2} l_d \tag{4}$$

$$w_i = -\frac{M_{i_1} l_d^2}{2(EI)_i} + \frac{S_i l_d^3}{6(EI)_i} + \frac{K_{BA_i} P_{i_2} l_d^2}{2} \qquad i = 1, \ldots, n \tag{5}$$

where $EI$ refers to the bending rigidity, and $K_{BA}$ refers to the bending–extension coupling constant arising from unsymmetric laminates. All other variables are defined in Fig. 1. The bending–extension coupling constant is calculated as

$$K_{BA} = b_{22}/c \tag{6}$$

where $b_{22}$ is an element of the sublaminate compliance matrix and $c$ is the beam width.[6]

When the deflections and gradients calculated in Eqs. (4) and (5) are equated and Eqs. (1) and (2) are used, an equation for the shear force acting on any one sublaminate can be derived:

$$S_j = \frac{(EI)_j S}{\sum_{i=1}^{n}(EI)_i}, \qquad j = 1, \ldots, n \tag{7}$$

To find the bending moment acting on the sublaminates, the force needed to align the endfaces of each sublaminate must be calculated. The displacement needed to align each face $\Delta$ is dependent on the gradient at its end (see Fig. 2), giving, for two adjacent sublaminates,

$$\Delta = -(\bar{z}_i - \bar{z}_{i+1})w' = \frac{P_{i_2} l_d}{(EA)_i} - \frac{P_{i+1_2} l_d}{(EA)_{i+1}}, \qquad i = 1, \ldots, n \tag{8}$$

where $EA$ refers to the sublaminate axial stiffness. Therefore,

$$\frac{P_{i+1_2} l_d}{(EA)_{i+1}} = \frac{P_{i_2} l_d}{(EA)_i} + (\bar{z}_i - \bar{z}_{i+1})w_i', \qquad i = 1, \ldots, n \tag{9}$$

By substituting Eq. (4) into Eq. (9) and simplifying, this gives the force necessary to align the endfaces:

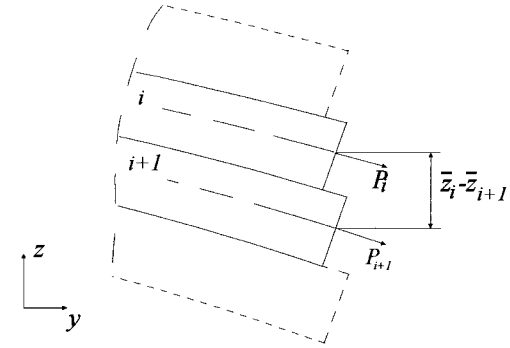


**Fig. 2 Endfaces of two sublaminates $i$ and $i+1$, showing difference in lengths due to gradient.**

$$P_{i_2} = -\sum_{j=1}^{n}(EA)_j(\bar{z}_i - \bar{z}_j)\left[-\frac{M_{i_1}}{(EI)_i} + \frac{S_i l_d}{2(EI)_i}\right] \Bigg/ \sum_{j=1}^{n}\left[\frac{(EA)_j}{(EA)_i} + (EA)_j(\bar{z}_i - \bar{z}_j)K_{BA_i}\right], \qquad i = 1, \ldots, n \tag{10}$$

With this equation, and by the substitution of Eqs. (4), (5), (7), and (1), an expression for the moment acting at the root of any sublaminate can be found:

$$M_{i_1} = \left\{M_1 + \frac{S_i l_d}{2(EI)_i}\left[\frac{A_i B_i}{C_i} - D_i\right]\right\} \Bigg/ \frac{1}{(EI)_i}\left[\frac{A_i B_i}{C_i} + E_i\right] \qquad i = 1, \ldots, n \tag{11}$$

where

$$A_i = \sum_{j=1}^{n}(EA)_j(\bar{z}_i - \bar{z}_j)$$

$$B_i = \sum_{j=1}^{n}\left(\left[\frac{1}{(EA)_i} + (\bar{z}_i - \bar{z}_j)K_{BA_i}\right] \times [(EA)_j\bar{z}_j + (EI)_j K_{BA_j}(EA)_j] - (EI)_j K_{BA_i}\right)$$

$$C_i = \sum_{j=1}^{n}\left[\frac{(EA)_j}{(EA)_i} + (EA)_j(\bar{z}_i - \bar{z}_j)K_{BA_i}\right]$$

$$D_i = \sum_{j=1}^{n}(EA)_j(\bar{z}_i - \bar{z}_j)[\bar{z}_j + (EI)_j K_{BA_j}]$$

$$E_i = \sum_{j=1}^{n}\{(EI)_j - (EA)_j(\bar{z}_i - \bar{z}_j)[(EI)_j K_{BA_j} + \bar{z}_j]\}$$

With these results, the tip deflection due to the bending of the delaminated beam ($\delta_{b_{\text{delam}}}$) is now calculated. With reference to Fig. 3, it is assumed that the difference between the bending deflection of the delaminated beam and the equivalent undelaminated beam, $\delta_{b_{\text{no-delam}}}$, is due to the loss in stiffness caused by delamination. The shear deflection of the undelaminated beam $\delta_{s_{\text{no-delam}}}$ is now also included, which ensures the correct value for $\delta_{s_{\text{delam}}}$ as the delamination approaches the top or bottom surface of the laminate (and, hence, as $\delta_{b_{\text{delam}}}$ approaches $\delta_{b_{\text{no-delam}}}$). The deflection of the delaminated beam due to shear, $\delta_{s_{\text{delam}}}$, is, therefore, defined as

$$\delta_{s_{\text{delam}}} = \delta_{b_{\text{delam}}} - \delta_{b_{\text{no-delam}}} + \delta_{s_{\text{no-delam}}} \tag{12}$$

When the standard result for the shear deflection of a tip-loaded cantilever beam is applied as found in many reference books (see, for example, Ref. 7), an approximate value for the effective shear rigidity of the delaminated section is given by

$$(AG)' = \tfrac{8}{15}\left(Sl_d \Big/ k^2 \delta_{s_{\text{delam}}}\right) \tag{13}$$

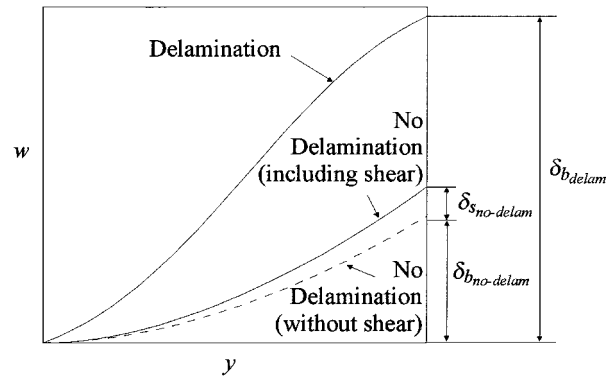


**Fig. 3 Comparison of delaminated and undelaminated deflected shapes for a tip-loaded cantilever.**

where $k$ is the shear correction factor for the cross section (which for a rectangular cross section is $\frac{2}{3}$) and $(AG)'$ is the reduced shear rigidity. The bending rigidity, torsional rigidity, and bending–torsion coupling needed in Eqs. (1–5) are calculated using well-known classical laminate analysis, together with the high aspect ratio plate model formulated by Weisshaar and Foist.[8] The torsional rigidity is assumed to be unchanged by delamination, and is, therefore, calculated for the undelaminated cross section. This limiting assumption means that only the bending modes of vibration can be used in the damage location procedure and that the bending–torsion coupling of the laminate must be small.

Because the calculation of shear rigidity is based on the static deflection of a delaminated beam, no account has been taken of the nonlinearity of the dynamic motion of a delaminated beam. This is due to the differential stretching effect of the sublaminates as the amplitude of vibration alters and is more apparent for delaminations creating sublaminates with high slenderness ratios.[9] The static approximation outlined in this paper is, therefore, more suitable for small delamination sizes or thick laminates.

#### Optimization: Structural Characterization

The first stage in locating damage within the laminate involves updating the initial undamaged DSM model so that it accurately describes the dynamic behavior of the system. This is achieved using the modified method of feasible directions (MMFD) within the program DOT, with the sensitivities calculated internally using forward differences.[10] The optimization problem is formally stated as follows.

Minimize the objective function:

$$O(\boldsymbol{X}) \tag{14}$$

subject to the inequality constraints

$$G_j(\boldsymbol{X}) \le 0, \qquad j = 1, \ldots, n_{\text{con}} \tag{15}$$

and the side constraints

$$X_i^L \le X_i \le X_i^U, \qquad i = 1, \ldots, n_{\text{dv}} \tag{16}$$

The objective function gives a measure of the fitness of the design and is defined as

$$O(\boldsymbol{X}) = \alpha \sum_i^{n_f} \left\{ 100 \times \left[ \frac{\omega_i^* - \omega_i(\boldsymbol{X})}{\omega_i^*} \right] \right\}^2 + \beta \sum_i^{n_f} \sum_j^{n_p} \left[ \phi_{ij}^* - \phi_{ij}(\boldsymbol{X}) \right]^2 \tag{17}$$

where $\omega_i(\boldsymbol{X})$ are the $n_f$ natural frequencies calculated using the DSM for a particular vector of design variables $\boldsymbol{X}$ and $\omega_i^*$ are the experimental frequencies. The constants $\alpha$ and $\beta$ are supplied by the user to ensure a well-conditioned objective function. Also, $\phi_{ij}(\boldsymbol{X})$ and $\phi_{ij}^*$ are the equivalent mode shapes defined at $n_p$ points along the beam.

It is assumed that the material properties supplied initially can be changed by 50% of their original value by the optimizer, so that the first nine design variables give the updated nine mutually independent material properties of a ply, as follows:

$$E_1^q = [1 + 0.5(2X_1 - 1)]E_1, \qquad E_2^q = [1 + 0.5(2X_2 - 1)]E_2$$
$$E_3^q = [1 + 0.5(2X_3 - 1)]E_3, \qquad \nu_{12}^q = [1 + 0.5(2X_4 - 1)]\nu_{12}$$
$$\nu_{23}^q = [1 + 0.5(2X_5 - 1)]\nu_{23}, \qquad \nu_{31}^q = [1 + 0.5(2X_6 - 1)]\nu_{31}$$
$$G_{12}^q = [1 + 0.5(2X_7 - 1)]G_{12}, \qquad G_{13}^q = [1 + 0.5(2X_8 - 1)]G_{13}$$
$$G_{23}^q = [1 + 0.5(2X_9 - 1)]G_{23} \tag{18}$$

where the superscript $q$ refers to the updated value for iteration $q$.

The boundary conditions at the root of the cantilever beam are modeled as three springs, with vertical displacement $h$, bending angle $\theta$, or torsional angle $\psi$ freedoms. The spring constants are given the values $k_h$, $k_\theta$, and $k_\psi$, respectively. Each stiffness constant was allowed to vary from a value of 1 to $1 \times 10^9$, using a logarithmic scale, as follows:

$$k_h^q = 10^{9X_{10}}, \qquad k_\theta^q = 10^{9X_{11}}, \qquad k_\psi^q = 10^{9X_{12}} \tag{19}$$

In all tests, the problem had no inequality constraints, removing Eq. (15).

#### Optimization: Detection of Delaminations

Once the analytical model of the undamaged beam matched the experimental data, the beam was damaged, and a numerical optimization technique was used to locate the damage.

The objective function for this process is the same as for the structural characterization stage, defined in Eq. (17).

The definition of the design variables is dependent on which of the optimization techniques are being used. For the MMFD, the design variables are the length and location of the delaminations. The number of delaminations and the position of the delaminations through the thickness of the laminate must be specified at the beginning of the optimization. This is because these variables can only take a finite number of values, that is, they are discrete design variables.

With reference to Fig. 4, if there is only one delamination, the design variables are

$$X_1 = l_a/l, \qquad X_2 = l_d/l \tag{20}$$

The design variables are encoded such that, effectively, the lower bound of the design variable ensures that the delamination starts after $Y = 0$:

$$X_1^L = X_2/2 \tag{21}$$

Also, an inequality constraint ensures that the sum of the delamination length and the location of the delamination does not exceed the total length of the beam:

$$G(\boldsymbol{X}) = (X_1/2) + X_2 - 1 \le 0 \tag{22}$$

An optimization run is carried out for each vertical ply location and where appropriate for each chosen number of delaminations.

The GA used in this research is the program GENESIS.[11] This is designed to allow a user-defined subroutine to be the evaluation function. If the GA is being used, the number and vertical position of the delaminations need not be specified at the beginning of

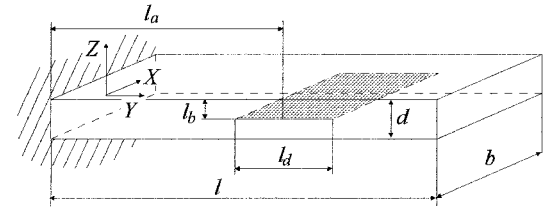


**Fig. 4 Cantilever beam with a single delamination.**

the optimization. This is because the design variables are encoded as a binary gene, which is inherently a discrete value, the desired numerical accuracy of the solution defining the length of the gene.

Hence, a third design variable, which defines the vertical position of the delamination, can be specified. Again, with reference to Fig. 4,

$$X_3 = l_b/d \tag{23}$$

Similarly, the number of delaminations and the extra design variables necessary to define them can be encoded simply by increasing the size of binary gene to include the extra information.

To ensure that the sum of the delamination size plus the delamination location is not larger than the length of the beam, a penalty function was introduced. This performs the same function as the inequality constraint in the gradient-based optimization, but is achieved by adding terms to the objective function when the design is in an unfeasible region. For a single delamination, the objective function becomes

$$O'(\boldsymbol{X}, r) = O(\boldsymbol{X}) + P[G(\boldsymbol{X})] \tag{24}$$

where the prime denotes the transformed objective function. The penalty function $P[G(\boldsymbol{X})]$ is a quadratic loss function, given by

$$P[G(\boldsymbol{X})] = r(\max\{0, G(\boldsymbol{X})\})^2 \tag{25}$$

where $r$ is a scalar chosen by the user and $G(\boldsymbol{X})$ is the constraint given in Eq. (22).

## Experimental Methodology

To assess the effectiveness of the damage detection methodology, a series of experimental tests for composite cantilever beams with simulated delaminations, created by inserting thin strips of PTFE film between layers during the manufacturing process, was carried out. The beams were manufactured from Hexcel Fiberdux T300/913C carbon-fiber/epoxy laminate with a nominal volume fraction of 60%, giving material properties of

$$E_1 = 138 \times 10^9 \text{ Pa}, \qquad E_2 = E_3 = 9.65 \times 10^9 \text{ Pa}$$

$$G_{12} = G_{13} = 1.07 \times 10^9 \text{ Pa}, \qquad G_{23} = 5.35 \times 10^8 \text{ Pa}$$

$$\nu_{12} = \nu_{13} = \nu_{23} = 0.263$$

$$\rho = 1787 \text{ kg/m}^3, \qquad t_{\text{ply}} = 0.125 \text{ mm}$$

The manufactured length of the beams was 400 mm, so that the first 100 mm of each beam could be clamped between two steel plates using four bolts. The steel plates were then secured to a steel table using a G clamp. The beams, therefore, had an exposed length $l$ of 300 mm, a width $b$ of 50 mm, and a nominal thickness $d$ of 1 mm.

Table 1 shows the laminate geometry of the beams and the size and location of the delaminations. One undelaminated beam was also manufactured for each layup.

An accelerometer with a frequency range of 0–600 Hz (Entran, Ltd., EGA-125-50D) was attached to one point of the beam with wax, after ensuring that the accelerometer did not lie on a nodal point of any of the modes. This measured acceleration in the $Z$ direction. The beams were excited with an impact hammer at different excitation points. Each point was excited three times, and an average was taken. The vertical impact force was measured with a force transducer (Brüel and Kjær; B and K 8200), and this force signal was used to trigger the recording of the data. The data were recorded using a Data Physics Corporation SignalCalc Ace frequency analyzer, and a frequency response function (FRF) was derived. A diagram of the clamping arrangement and the experimental equipment is shown in Fig. 5.

**Table 1 Description of the experimental beams**

| Case | Layup, deg | $X_1$ | $X_2$ | $X_3$ |
|---|---|---|---|---|
| 1 | $[0, 90]_{2,s}$ | 0.49 | 0.167 | 0.5 |
| 2 | $[0, 90]_{2,s}$ | 0.62 | 0.167 | 0.5 |
| 3 | $[0, \pm 45, 0]_s$ | 0.49 | 0.167 | 0.5 |
| 4 | $[0, \pm 45, 0]_s$ | 0.62 | 0.167 | 0.5 |
| 5 | $[0, \pm 45, 0]_s$ | 0.117 | 0.167 | 0.5 |
| 6 | $[0, \pm 45, 0]_s$ | 0.117 | 0.167 | 0.25 |

Once an FRF was obtained for each point, the commercially available package Star System used a curve fitting process to determine the frequency and peak amplitude for each of the points.[12] With the gain and phase information for each of the points, an animation could then be produced for each natural frequency, from which it is possible to ascertain the type of mode being displayed.

## Results

### Experimental Results

Table 2 shows the first four bending frequencies of the undelaminated beams. These were obtained from the average of the results from five tests.

A useful way of comparing mode shapes is the modal assurance criterion (MAC), which is a scalar quantity. When comparing a mode shape $i$ with mode shape $j$, the MAC is defined as[13]

$$\text{MAC} = \frac{\left(\boldsymbol{\phi}_i^T \boldsymbol{\phi}_j\right)^2}{\left(\boldsymbol{\phi}_i^T \boldsymbol{\phi}_i\right)\left(\boldsymbol{\phi}_j^T \boldsymbol{\phi}_j\right)} \tag{26}$$

where $\boldsymbol{\phi}_i$ and $\boldsymbol{\phi}_j$ are the mode shapes of mode $i$ and $j$, respectively, and the superscript $T$ denotes vector transposition. A MAC of 1 denotes a perfect correlation between two mode shapes, whereas a MAC of 0 signifies no correlation.

Table 3 shows the average of the experimental bending frequencies normalized with respect to the average undelaminated frequencies $\bar{\omega}$ for delaminated cases 1, 2, and 3 and the MAC for each mode when compared to the equivalent undelaminated mode shapes. Table 4 shows the equivalent results for cases 4, 5, and 6.

The greatest drop in natural frequency occurs when the delamination lies in a location of high shear force in a particular mode.[14] Figure 6 shows the frequency drop for a $1 \times 0.1 \times 0.01$ m aluminum beam with a 15% delamination ($X_2 = 0.15$, $X_3 = 0.5$), produced by the DSM. It can be seen that for a cantilever beam, the greatest frequency drop occurs near the root for all of the modes and at regions

**Table 2 Undelaminated beam bending frequencies**

| Layup | $[0, 90]_{2,s}$, deg | $[0, \pm 45, 0]_s$, deg |
|---|---|---|
| 1B/[Hz] | $14.45 \pm 0.38$ | $14.20 \pm 0.12$ |
| 2B/[Hz] | $91.28 \pm 0.29$ | $88.25 \pm 0.17$ |
| 3B/[Hz] | $250.79 \pm 0.81$ | $242.58 \pm 1.33$ |
| 4B/[Hz] | $486.03 \pm 1.48$ | $482.12 \pm 1.85$ |

**Table 3 Normalized bending frequencies and MAC for cases 1–3**

| | Case 1 | | Case 2 | | Case 3 | |
|---|---|---|---|---|---|---|
| Mode | $\bar{\omega}$ | MAC | $\bar{\omega}$ | MAC | $\bar{\omega}$ | MAC |
| 1B | 0.92 | 0.98 | 0.97 | 0.97 | 1.00 | 0.88 |
| 2B | 0.95 | 1.00 | 0.99 | 0.99 | 0.99 | 1.00 |
| 3B | 0.85 | 0.92 | 0.96 | 0.99 | 0.99 | 0.99 |
| 4B | 0.95 | 0.98 | 0.85 | 0.83 | 0.98 | 1.00 |

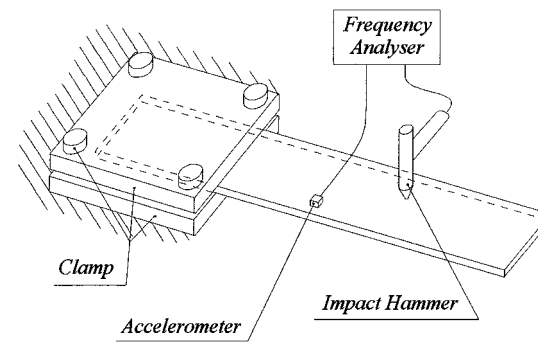


**Fig. 5 Schematic arrangement of experimental beams.**

**Table 4 Normalized bending frequencies and MAC for cases 4–6**

| | Case 4 | | Case 5 | | Case 6 | |
|---|---|---|---|---|---|---|
| Mode | $\bar{\omega}$ | MAC | $\bar{\omega}$ | MAC | $\bar{\omega}$ | MAC |
| 1B | 0.96 | 0.98 | 0.97 | 0.98 | 0.97 | 0.99 |
| 2B | 0.99 | 0.99 | 0.95 | 1.00 | 0.93 | 0.98 |
| 3B | 0.99 | 0.98 | 0.93 | 0.99 | 0.91 | 0.99 |
| 4B | 0.97 | 0.97 | 0.92 | 0.97 | 0.89 | 0.98 |

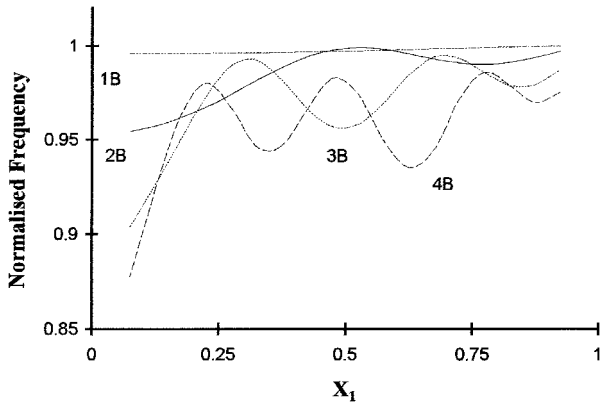


**Fig. 6 Normalized bending frequencies for an aluminum beam with a delamination at different axial locations.**

of high change in curvature. In the case of the experimental beam results, a significant frequency drop can be seen for some cases, most notably the third bending mode for case 1 and the fourth bending modes for cases 2, 5, and 6.

The MAC also show that the mode shapes have been affected for these modes, although less so than for the natural frequencies. There is also more experimental scatter on the individual points of the mode shapes, due to the difficulty of achieving a high repeatability of impacts during the modal testing.

A higher error was also noticed for the fundamental bending mode. This is because the natural frequency of the fundamental mode is low compared to the frequency range of the experiment, causing errors due to low resolution.

### Structural Characterization

In the structural characterization stage, experimental frequencies and mode shapes for the undamaged beams are used to quantify the material properties and boundary conditions. It was envisioned that, for this stage, the structure would remain fixed to its support during its life and that any damage would occur in situ. However, because the delaminations were produced artificially, the boundary conditions change for each beam and, therefore, between the undamaged and damaged cases. Hence, the structural characterization was carried out only for the undamaged $[0, 90]_{2,s}$ deg beam, and it was assumed that the material properties and support stiffnesses remained similar throughout the remainder of the experimental tests.

The objective function was formulated with $\alpha = 1.0$ and $\beta = 50.0$, which meant that the frequency and mode parts of the objective function were approximately the same size at convergence. Also, the mode shapes were quantified at five ($n_p = 5$) points, which were 20, 40, 60, 80, and 100% along the length of the beam. Because of the uncertainty of the accuracy of mode 1, a weighting factor of 0.8 was used on this mode.

After the optimization run, the final values of the design variables were

$$X_7 = X_8 = X_9 = X_{10} = 1.0 \text{ (upper bounds)}$$

$$X_3 = X_5 = X_6 = 0.5 \text{ (unchanged)}$$

$$X_1 = 0.64, \qquad X_2 = 0.39, \qquad X_4 = 0.63, \qquad X_{11} = 0.75$$

$$X_{12} = 0.56 \text{ (unchanged)}$$

**Table 5 Initial and final optimizer frequencies for the $[0, 90]_{2_s}$, deg beam**

| | DSM frequency, Hz | |
|---|---|---|
| Mode | Initial | Final |
| 1B | 14.01 | 14.92 |
| 2B | 87.46 | 93.16 |
| 3B | 235.86 | 251.15 |
| 4B | 432.36 | 460.24 |

To increase the frequencies closer to the experimental values, Young's modulus in the fiber direction ($X_1$) had increased, as well as the two spring constants in the bending direction $k_h$ and $k_\theta$ ($X_{10}$ and $X_{11}$). The shear moduli $G_{13}$ and $G_{23}$ ($X_8$ and $X_9$) also increased to their upper bounds, increasing the shear rigidity of the 0- and 90-deg layers. The major Poisson's ratio also increased, increasing stiffness of the laminate, although this effect is small. Because there is no bending–torsion coupling for this laminate, it is unclear why $G_{12}(X_7)$ increased.

Because the experimental torsion modes were not included in the objective function, the torsional spring constant remained unchanged throughout the optimization. The two springs stiffnesses in the bending directions, however, increased, showing that the clamping arrangement stiffness was sufficient to justify the cantilever beam assumptions. It was, therefore, decided to use spring constant values of $1 \times 10^9$ N/m, $1 \times 10^9$ Nm/rad, and $1 \times 10^9$ Nm/rad for $k_h$, $k_\theta$, and $k_\psi$, respectively (effectively cantilever boundary conditions), and to carry out the characterization process again with the spring stiffness values constant.

The initial and final frequencies with the boundary conditions constant are shown in Table 5, showing a better correlation with the experimental frequencies given in Table 2.

Note that the final material properties obtained by this procedure may not be the actual material properties. The updated material properties are used to reduce the errors in the analytical model and may be accounting for deficiencies in the model. For instance, there may be some anticlastic bending in the experimental beams, which increases the effective stiffness of the beams, and would be interpreted as a higher bending stiffness by the optimizing procedure.

### Locating Delaminations Using a Gradient Technique

With the characterized material properties, the frequencies and mode shapes were then used to locate the delaminations using the gradient-based optimization procedure. Because locating a delamination is a discrete optimization problem, an optimization run must be carried out for every ply location and the minimum objective function used to denote the correct location. To simplify this process, it was decided that the number of possible delaminations would be restricted to one. For the eight-ply laminates used, restricting the number of possible delaminations to one means that the optimizer must be run seven times.

For cases 1–6, and using the new material properties, the gradient-based optimization method was applied to each layer. To ensure that a global minimum was found for each case, three starting positions were used. These were $X_1 = 0.25$, $X_2 = 0.3$; $X_1 = 0.5$, $X_2 = 0.3$; and $X_1 = 0.75$, $X_2 = 0.3$. The optimizer control parameters and constants used to derive the objective function were identical to those used for the characterization stage.

It is helpful to visualize the design space of the problem, and a two-dimensional representation is possible if the problem is restricted to two design variables. If the starting $Z$ position of the (single) delamination is specified at the beginning of the optimization, the problem remains relatively simple and can be shown graphically. When multiple combinations of delamination size and horizontal location are tried, lines of constant objective function can be calculated. This is shown for case 1 in Fig. 7. It appears from Fig. 7 that the objective function is much more influenced by the size of delamination $X_2$ than its position $X_1$ because the gradient in the objective function is much steeper for this design variable. This is because the shear rigidity is a function of the inverse of the square of the delamination length, so that the shear rigidity drops sharply with increasing

**Table 6 Final optimizer solution of delamination location and size, created by the gradient-based optimizer method**

| Case | $X_1$ (difference) | $X_2$ (difference) | $X_3$ (difference) | Objective function |
|---|---|---|---|---|
| 1 | −0.025 | 0.006 | 0.0 | 138.2 |
| 2 | −0.073 | −0.001 | 0.0 | 57.9 |
| 3 | −0.085 | −0.054 | −0.375 | 23.4 |
| 4 | 0.064 | −0.050 | −0.25 | 27.3 |
| 5 | 0.027 | −0.030 | −0.125 | 21.8 |
| 6 | 0.086 | 0.063 | −0.125 | 31.6 |

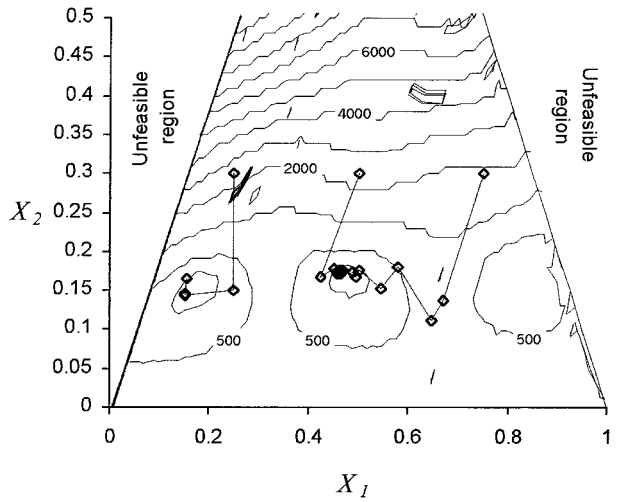


**Fig. 7 Two-dimensional design space created by a single delamination (case 1).**

delamination size. Note from Fig. 7 that there are three points where the objective function is locally at a minimum.

Also shown in Fig. 7 is the variation of the objective function with iteration, starting from the three initial delamination locations, using DOT. For two positions, the delamination has been located to within 5% of its actual location and 4% of its size. However, for the third starting position, the delamination has not been located accurately. This shows that care must be taken to ensure that a global optimum is located when using the gradient-based optimizing procedure.

Table 6 shows the final results for the six experimental cases, in terms of the difference from the actual result. The difference is calculated by

$$X_i(\text{difference}) = X_i(\text{optimized}) - X_i(\text{experimental})$$

$$i = 1, \ldots, 3 \quad (27)$$

Because the laminates have eight plies, these results are obtained by finding the lowest value of objective function from running an optimization starting at each of the seven-ply interfaces.

Overall, the differences in the horizontal location $X_1$ and delamination size $X_2$ remained reasonably low, but the vertical location $X_3$ was not located well. The delamination size was also consistently underestimated for cases 3–5, and this can perhaps be attributed to resin leakage during curing, reducing the delamination size. On average, it took approximately 700 function calls to locate the damage.

#### Locating Delaminations Using a GA

Table 7 shows the best solution of delamination size and location for the experimental damaged beams produced by the GA. To produce these solutions, a gene containing the three design variables encoded to four decimal places was used, giving a gene of 23 bits in length. The control parameters were population size = 40, probability of mutation = 0.001, and probability of crossover = 0.8. The scaling window was the preceding five generations.

Note that in most cases the GA has resulted in delaminations being located with better accuracy than the gradient-based method because it is a global search routine. The GA has consistently produced

**Table 7 Final optimizer solution of delamination location and size, created by the GA**

| Case | $X_1$ (difference) | $X_2$ (difference) | $X_3$ (difference) | Objective function |
|---|---|---|---|---|
| 1 | −0.024 | 0.006 | 0.0 | 138.2 |
| 2 | 0.029 | 0.054 | −0.375 | 59.9 |
| | (0.008)[a] | (−0.010) | (0.0) | (4.0) |
| 3 | 0.363 | −0.056 | −0.125 | 15.3 |
| | (−0.099) | (−0.074) | (−0.25) | (0.3) |
| 4 | 0.157 | −0.023 | −0.375 | 23.0 |
| 5 | 0.003 | −0.006 | 0.0 | 10.3 |
| 6 | 0.098 | 0.048 | −0.125 | 25.4 |

[a]Parentheses indicate that no mode shapes were used in the optimization.

a value of objective function that is less than (or approximately equivalent to, in cases 1 and 2) those produced by the gradient-based algorithm. This is especially noticeable for case 5, when a much better solution has been found by the GA.

However, note that, for $X_2$ and $X_3$ for case 2 and $X_1$ for cases 3 and 4, the GA has converged to a worse solution than did the gradient-based method. In these cases the gradient-based optimizer had benefited from a local minima caused by starting very close to its final position. However, the objective functions produced by the GA are lower than (cases 3 and 4) or equivalent to (case 2) those produced by the gradient method, showing that, in fact, the GA solutions are probably the global ones. For these cases, the optimization was also run without the mode shapes influencing the objective function. A much better solution was found for case 2, as was a better solution for delamination position for case 3 (also shown in Table 7), showing that the errors in the solution were caused by the significant errors inherent in measuring experimental mode shapes.

This increase in accuracy obtained by using the GA has, however, been achieved at the expense of efficiency. On average, the GA took approximately 1500 function calls to achieve a solution.

## Conclusions

An analytical model of a delaminated beam has been developed. This uses the DSM to produce the undamped frequencies and mode shapes of a delaminated beam. The delaminated area is assumed to be modeled by a reduced shear rigidity. The shear rigidity of a delaminated beam is calculated using a static beam model.

It was seen that using this model, a 1-cm delamination reduces the shear rigidity to over $\frac{1}{100}$ of its original value for some layups. Applied to the dynamic model, this reduction in shear rigidity produced reductions in frequency. This drop was seen to be larger if the delamination was in a region of high shear force for a particular mode and was also larger for modes with a higher order.

A two-stage damage location procedure was developed. The first stage was structural characterization, where the errors in the analytical model of an undelaminated beam were minimized. This used a gradient-based optimization technique, which minimized the difference between the frequencies and mode shapes produced by the analytical model and those obtained by experiment. The second stage was to locate the delaminations, using either a gradient-based optimization technique or a GA.

This methodology was validated by experiment. PTFE strips were inserted between the layers of carbon-fiber/epoxy beams, creating known delaminations. Experimental results showed drops in frequency of up to 15%.

With these experimental results, the delaminations were successfully located by both the gradient-based method and the GA. It was seen that the horizontal position of delaminations was identified with more accuracy than either its size or its vertical position. In most cases, the GA located a better solution than the gradient-based method, shown by a lower value in objective function. However, because of experimental inaccuracy, the global minimum sometimes corresponded to a different delamination location when compared with the experimental beam. The ability of the GA to locate a global minimum came at the expense of computer efficiency.

## Acknowledgments

This work was carried out as Ph.D. research at the University of Bath under sponsorship by the Engineering and Physical Sciences Research Council, Studentship Number 96306367. The authors would also like to thank the Department of Engineering and Applied Science at the University of Bath for their assistance in the manufacture of the experimental laminates.

## References

[1]Cawley, P., and Adams, R. D., "A Vibration Technique for Non-Destructive Testing of Fibre Composite Structures," *Journal of Composite Materials*, Vol. 13, April 1979, pp. 161–175.

[2]Hajela, P., and Soeiro, F. J., "Structural Damage Detection Based on Static and Modal Analysis," *AIAA Journal*, Vol. 28, No. 6, 1990, pp. 1110–1115.

[3]Ruotolo, R., and Surace, C., "Damage Assessment of Multiple Cracked Beams: Numerical Results and Experimental Validation," *Journal of Sound and Vibration*, Vol. 206, No. 4, 1997, p. 567.

[4]Okafor, A. C., Chandrashekhara, K., and Jiang, Y. P., "Damage Detection in Composite Laminates with Built-in Piezoelectric Devices Using Modal Analysis and Neural Network," *Smart Structures and Materials: Smart Sensing, Processing and Instrumentation*, edited by W. B. Spillman, *SPIE Proceedings*, Vol. 2444, 1995, pp. 314–325.

[5]Banerjee, J. R., and Williams, F. W., "Exact Dynamic Stiffness Matrix for Composite Timoshenko Beams with Applications," *Journal of Sound and Vibration*, Vol. 194, No. 4, 1996, pp. 573–585.

[6]Tsai, W., and Hahn, H. T., *Introduction to Composite Materials*, Technomic, Westport, CT, 1980.

[7]Ryder, G. H., *Strength of Materials*, Macmillan, London, 1969, p. 171.

[8]Weisshaar, T. A., and Foist, B. L., "Vibration Tailoring of Advanced Composite Lifting Surfaces," *Journal of Aircraft*, Vol. 22, No. 2, 1985, pp. 141–147.

[9]Lestari, W., Lu, X., and Hanagud, S., "Dynamics of a Delaminated Beam: Effects of Nonlinearity," AIAA Paper 2000-1505, April 2000.

[10]*DOT Users Manual*, VMA Engineering, Vanderplats Research and Development, Inc., Colorado Springs, CO, 1995.

[11]Grefenstette, J. J., "A User's Guide to GENESIS," 1990; URL: ftp://ftp.aic.nrl.navy.mil/pub/galist/src/ [cited 22 September 1994].

[12]"STAR System Users Guide," Spectral Dynamics, Inc., San Jose, CA, 1994.

[13]Ting, T., Chen, T. L. C., and Twomey, W., "Correlating Mode Shapes Based on the Modal Assurance Criterion," *Finite Elements in Analysis and Design*, Vol. 14, No. 4, 1993, pp. 353–360.

[14]Tracy, J. J., and Pardoen, G. C., "Effect of Delamination on the Natural Frequencies of Composite Laminates," *Journal of Composite Materials*, Vol. 23, Dec. 1989, pp. 1200–1215.

A. N. Palazotto
*Associate Editor*